View Article Online
View Journal

Faraday Discussions

Accepted Manuscript

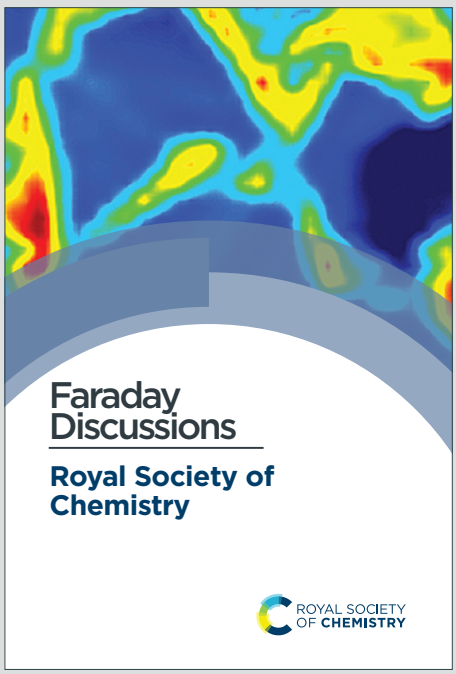

This is an Accepted Manuscript, which has been through the Royal Society of Chemistry peer review process and has been accepted for publication.

Accepted Manuscripts are published online shortly after acceptance, before technical editing, formatting and proof reading. Using this free service, authors can make their results available to the community, in citable form, before we publish the edited article. We will replace this Accepted Manuscript with the edited and formatted Advance Article as soon as it is available.

You can find more information about Accepted Manuscripts in the Information for Authors.

Please note that technical editing may introduce minor changes to the text and/or graphics, which may alter content. The journal's standard Terms & Conditions and the Ethical guidelines still apply. In no event shall the Royal Society of Chemistry be held responsible for any errors or omissions in this Accepted Manuscript or any consequences arising from the use of any information it contains.

This article can be cited before page numbers have been issued, to do this please use: S. Herres-Pawlis, J. Ke, N. Conen, F. Latz, J. N. Neumann, M. Fuchs, A. Hoffmann and A. Jupke, *Faraday Discuss.*, 2025, DOI: 10.1039/D5FD00062A.

ROYAL SOCIETY OF CHEMISTRY

www.rsc.org/faraday_d

View Article Online
DOI: 10.1039/D5FD00062A

Data Availability Statement

The data that supports the findings of this study are openly available in RADAR4chem at https://www.radar-service.eu/radar/en/dataset/qg2e8yckr7kjtj5b?token=ciIcXLyzxVecDszreuQy

The authors would further like to thank RADAR4Chem for support and funding of the repository.

Open Access Article. Published on 22 July 2025. Downloaded on 8/14/2025 4:27:06 AM.
This article is licensed under a Creative Commons Attribution 3.0 Unported Licence.

Faraday Discussions Accepted Manuscript

Title

Unleashing the Power of Non-Toxic Zn-Guanidine Catalysts for Sustainable Lactide Polymerization through Smart Modeling

View Article Online
DOI: 10.1039/D5FD00062A

Author List

Jinbo Ke[a, ‡], Niclas Conen[b, ‡], Filip Latz[b], Jan Niclas Neumann[a], Dr. Martin Fuchs[a], Dr. Alexander Hoffmann[a], Prof. Dr. Andreas Jupke[*b] and Prof. Dr. Sonja Herres-Pawlis[*a]

Address

[a]: Institute of Inorganic Chemistry, RWTH Aachen University, Landoltweg 1A, 52074 Aachen, Germany, E-mail: sonja.herres-pawlis@ac.rwth-aachen.de

[b]: Fluid Process Engineering (AVT.FVT), RWTH Aachen University, Forckenbeckstraße 51, 52074 Aachen, Germany, E-mail: andreas.jupke@avt.rwth-aachen.de

‡: These authors contributed equally to this work.

Open Access Article. Published on 22 July 2025. Downloaded on 8/14/2025 4:27:06 AM.
This article is licensed under a Creative Commons Attribution 3.0 Unported Licence.

Faraday Discussions Accepted Manuscript

Abstract

Polylactide (PLA) is one of the most promising bioplastics and is therefore often quoted as a solution to fight today's global plastics crisis. However, current PLA production via ring opening polymerization (ROP) of lactide is not yet sustainable since it heavily relies on the toxic catalyst tin octanoate. To overcome the hurdles in scale up and to accelerate the transition of promising new non-toxic alternative ROP catalysts from laboratory to industry, model-based analysis is a highly effective tool. Herein, our previously introduced kinetic model for the ROP of L-lactide using non-toxic and robust Zn guanidine "asme"-type catalyst under industrial relevant melt conditions is expanded upon two new co-initiators. The experimental data is evaluated using "traditional" kinetic analysis following pseudo first order kinetics to approximate a relationship between co-initiator concentration and the rate of polymerization. The range of validity of these findings is considerably expanded by taking model data into account to compare the performance of the different co-initiators in lactide ROP.

Introduction

Plastics have become indispensable across modern society due to their exceptional versatility, low-cost production, and adaptability to a wide range of applications. From packaging and construction materials to medical devices and electronics, plastics offer lightweight, durable, and mouldable solutions to countless industries.[1] However, these benefits come at a significant cost. Most conventional plastics are derived from non-renewable fossil resources and are resistant to natural degradation, leading to their persistent accumulation in terrestrial and marine environments.[2–4] Furthermore, growing evidence links microplastics to adverse health effects in both wildlife and humans, the long-term impact of which has yet to be determined.

In light of these challenges, PLA has emerged as a promising alternative to petroleum-based plastics. Derived from biological resources, PLA is biodegradable, biocompatible, and holds the potential to compete economically with conventional polymers.[5,6] Among the various synthesis routes, ring-opening polymerization (ROP) of lactide is the preferred method for PLA production. This approach allows for the generation of high molecular mass polymers with controlled tacticity and low dispersity, which are crucial for tailoring material properties.[7–9] Moreover, ROP proceeds without the need for solvents or by-product removal, thereby simplifying the downstream processing and reducing the environmental burden typically associated with polymer production.

View Article Online
DOI: 10.1039/D5FD00062A

Open Access Article. Published on 22 July 2025. Downloaded on 8/14/2025 4:27:06 AM.
This article is licensed under a Creative Commons Attribution 3.0 Unported Licence.

In industrial production of PLA, the metal complex catalysed ROP is the preferred procedure, and the produced polymer tacticity and its molar masse can be controlled.[7–9] Standardly, stannous octanoate ($Sn(Oct)_2$) combined with an alcohol (co-initiator) is used as the catalyst at industrial scale.[10] However, $Sn(Oct)_2$ is toxic, and traces remain in the polymer after ROP, which can be accumulated in the environment during biodegradation of PLA.[11–13] Therefore, the focus of ongoing research has been shifted to developing non-toxic metal-based catalysts. Numerous studies have been conducted that present non-toxic alternatives for ROP of lactide based on metals such as Mg, Al, Fe, Zn, Ge, Sc and others.[14–43] Among these catalysts, zinc-based systems are especially attractive, due to high activity, availability and low cost of Zn.[30,44–68] Various zinc-based catalysts have been reported to activate ROP of lactide, exceeding the activity of $Sn(Oct)_2$, but the required reaction conditions, additional solvents, low temperature, an inert atmosphere and a purified monomer feed, are at odds with industrial scale.[49,51,52,54,56,59–67,69–71] Therefore, robust, non-toxic and highly active catalysts are needed that can handle these industrially important requirements.[72] Herres-Pawlis et al. reported several robust Zn-based catalysts combined with various bis- and hybrid guanidine ligands used under industrially relevant conditions.[55,73–76] Besides the metal-based catalysts, co-initiators (Co-I) play an equally important role in the ROP of lactide on both lab and industry scale.[28,77,78] The deliberate addition of these external nucleophilic co-initiators leads to increased control of the molar mass of the polymer. Furthermore, due to the assistance of co-initiators, the synthesis of complicated polymer architectures and co-polymers is enabled.[49,77] Different types of alcohol with various lengths or branches have been described as co-initiators for the ROP of lactide.[28,43,49,77,79–86] For the industrial application of these catalysts combined with co-initiators, detailed model-based investigations of the behaviour of catalysts on lab scale is needed. Recently, we developed a mathematical model for describing the ROP of lactide catalyzed by “asme”-type zinc catalysts.[87] In literature, a second order rate law is commonly used to describe the ROP of lactide (eq. 1). Under the assumption that either a coordination-insertion mechanism (CIM) or an activated-monomer mechanism (AMM) takes place, this can be simplified to a pseudo-first order rate law (eq. 2), since in the ideal case, the catalyst concentration is constant in both mechanisms. This results in the following equations for the reaction rate (v) with [LA] being the concentration of the monomer, [Cat] the catalyst concentration, k_p the rate constant of polymerization, and the observable reaction rate constant k_{obs} as the product of [k_p] and [Cat].[76]

$$v = \frac{-\mathrm{d}[\mathrm{LA}]}{\mathrm{d}t} = k_p \times [\mathrm{Cat}] \times [\mathrm{LA}] \quad (1)$$

$$v = \frac{-\mathrm{d}[\mathrm{LA}]}{\mathrm{d}t} = k_{obs} \times [\mathrm{LA}] \quad (2)$$

Note, that in lactide ROP it is oftentimes not distinguished between catalyst and initiator and both terms are used synonymously in literature.[76] After integration and transformation of eq. 2 the linearized eq. 3 is obtained.

$$\ln\left(\frac{[\mathrm{LA}]_0}{[\mathrm{LA}]_t}\right) = k_{obs} \times t \quad (3)$$

As shown in **Figure 3**, this gives k_{obs} as the slope of the semilogarithmic plot of monomer consumption vs. the time ($\ln\left(\frac{[\mathrm{LA}]_0}{[\mathrm{LA}]_t}\right)$, t).

From the slope of a plot of the resulting k_{obs} vs. [Cat] the reaction rate constant k_p is then obtained, which allows for the comparison of the performance of different polymerization catalysts (**Figure 4**).

However, this textbook-like method has its limitations and does not cover phenomena during ROP that might decrease the reaction rate like initiation *via* ligands or catalyst decomposition.[84] Note, that it is also not possible to distinguish between CIM and AMM using this method and certain catalysts might promote both mechanisms simultaneously in concurrent reactions. As Fuchs further showed for lactide ROP with a Zn-guanidine catalyst, both the experimental effort

Faraday Discussions Accepted Manuscript

View Article Online
DOI: 10.1039/D5FD00062A

and the resource consumption necessary for classic kinetic analysis drastically increase if industrially active co-initiators are added to the reaction system.[87] Hence, a straight-forward method is needed to incorporate co-initiators into the kinetic analysis of lactide ROP to enable a translation of promising new, non-toxic catalysts from lab to industry. As demonstrated previously, due to the increased material investment of the described classical kinetic analysis, model-based methods are a much-needed tool to improve the multivariate understanding of the kinetics of such ROP catalysts (e.g. varying catalyst and initiator concentration, temperature etc.).[87]

Building on our approach for catalysing lactide ROP using non-toxic zinc-"asme" catalysts, this work expands both the experimental and modelling aspects of the catalytic system. Specifically, we introduce and investigate the use of bifunctional co-initiators carrying two hydroxyl groups, in contrast to the monofunctional variants employed previously. These bifunctional co-initiators enable the propagation reaction to proceed from both ends of the polymer chain, theoretically allowing for faster monomer conversion compared to using a mono-functional co-initiator. The influence of these bifunctional co-initiators on polymer growth will be systematically studied and incorporated into an expanded kinetic model, enabling a more precise, model-based description of the polymerization process. Ultimately, this advancement aims to broaden the applicability of our catalytic system under industrially relevant conditions while decreasing the amount of catalyst and improving control over key material characteristics, such as molecular mass and dispersity.

Experimental

Ring-Opening Polymerization of L-Lactide

In a glovebox (*MBRAUN*) L-lactide (8.0 g, 55.5 mmol), phenyl-1,4-dimethanol, if used as the co-initiator, and the catalyst were weighed according to the respective monomer-to-co-initiator-to-catalyst-ratio ([LA]/[co-I]/[Cat]-ratio). All exact weighed amounts are listed in **Table S1** in the supporting information. The solid reactants were combined and homogenized using an agate mortar. The mixture was transferred to a screw cap vial and removed from the glovebox. A stainless-steel reactor equipped with a precision overhead stirrer *("minisprint PRE1946 - Premex Reactor AG*, torque = 20 N cm), a Raman probe (sapphire lens, d = 0.1 mm) and a temperature probe were used for all polymerization experiments (see **Figure S1**). The polymerization was monitored *via* Raman spectroscopy using a *Kaiser Optical System RXN1* spectrometer with an *Invictus NIR Diode Laser* (wavelength 785 nm, 450 mW) combined with a *TE Cooled 1024 CCD Detecto*. The reactor was preheated to the reaction temperature of T = 150 °C for at least 1 h prior to the polymerization experiments and flushed with Ar (3x). The solid reaction mixture was transferred to reactor using Ar counter flow. If used as the co-initiator 1-hexanol was added to the reactor using a Hamilton syringe according to the respective [La]/[co-I]/[Cat]-ratio (**Table S1**-**S5**). The reactor was closed, and the Raman measurement was started which marks the start of the polymerization (t = 0). After the desired reaction time of 90 mins the measurement was stopped. The crude polymerization mixture was analysed using ^{1}H NMR spectroscopy to determine the polymer yield. For further analysis a sample of the crude product was dissolved in DCM (2.0 ml) and precipitated from EtOH (200.0 ml) and dried in high vacuum. The molar mass and the dispersity of the polymer was determined using a *Viscotek GPCmax VE-2001* system combined with a *VE-3580 refractive index detector* an HPLC pump and a *Viscotek 270 Dual Detector* viscosimeter. Two *Viscotek T colums* (Styrene-Divinylbenzene-Copolymer, pore size between 500 Å and 5000 Å) were used as the stationary phase. THF was used as the mobile phase at a flow rate of 1 ml min^{-1} with the sample concentration ranging between 5 to 7 g l^{-1}. A conventional calibration based on polystyrene standards was used. To access the molar mass of PLA the obtained molar masses were corrected by a factor of 0.58 according to literature.[88] The obtained Raman data was assessed using the software *Peaxact* (V4.0 or higher) by *S-PACT.* The characteristic

Open Access Article. Published on 22 July 2025. Downloaded on 8/14/2025 4:27:06 AM.
This article is licensed under a Creative Commons Attribution 3.0 Unported Licence.

Faraday Discussions Accepted Manuscript

signals of lactide (656 cm^{-1}) and PLA (872 cm^{-1}) were evaluated to determine the reaction rate constant of the polymerization (k_p) as described below.

View Article Online
DOI: 10.1039/D5FD00062A

Ring-Opening Polymerization of L-Lactide in Schlenk Tubes

In a glovebox (*MBRAUN*) L-lactide, *p*-methylbenzyl alcohol, used as the co-initiator, and zinc chloride, used as catalyst, were weighed depending on the monomer-to-co-initiator-to-catalyst-ratio ([LA]/[co-I]/[Cat]-ratio = 2500:10:1) and completely mixed in an agate mortar. The exact amounts are listed in **Table S1** in the supporting information. The solid mixture was divided evenly (approximately 500 mg per portion), and each portion was transferred into a Schlenk tube contained a magnetic stirrer (15 x 4.5 mm). Then the loaded Schlenk tube was heated in an oil bath (150 °C) and the stirring speed was set to 260 rpm. After the desired reaction time, the corresponding tube was removed from the oil bath and cooled under a water flow to stop the polymerization. To determine the polymer yield, the crude product was dissolved in DCM (2.0 mL), an aliquote was transferred to a NMR tube, dried under high vacuum, and a ^{1}H-NMR spectrum recorded.

Results and discussion

Classical analysis of the experimental results

Analogue to our previous study the "asme"-type complex [$ZnCl_2$(TMGasme)] (**C1**) was chosen as catalyst for lactide ROP. **C1** was resynthesized according to the literature procedure reported by Schäfer et al..[74]

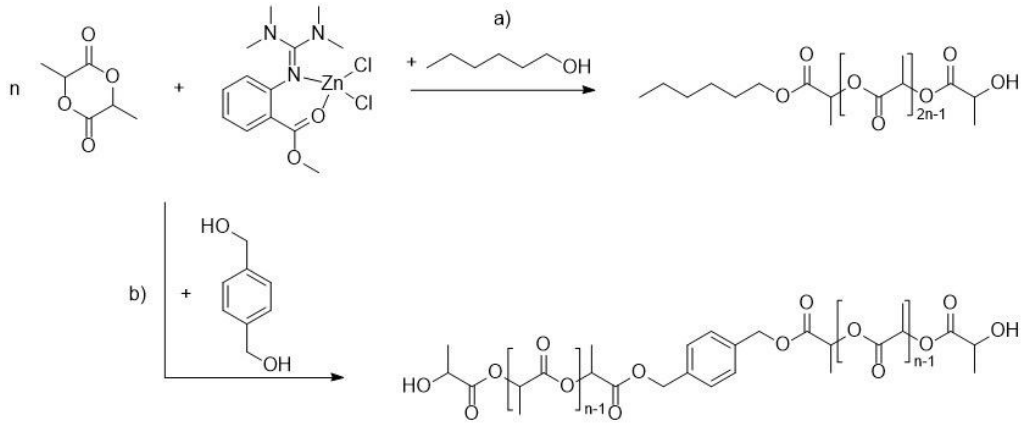

Scheme 1: Lactide ROP catalysed by [$ZnCl_2$(TMGasme)] (**C1**) with two different co-initiators: a) 1-hexanol (**CoI1**); b) 1,4-benzenedimethanol (**CoI2**)

To further expand our polymerization model, two very different alcohols were chosen as co-initiators for this study (**Scheme 1**). As guiding principles for the selection of co-initiators, we focused on the potential industrial application with cost and high molar mass of the PLA as indicators, as well as the handling of the co-initiator in the lab. 1-Hexanol (**CoI1**) was chosen as the first candidate, due to its low cost and boiling point of 157 °C which ensures reliable lab scale testing at 150 °C (see Experimental). As a second candidate we selected 1,4-benzenedimethanol (**CoI2**). Due to its solid state of aggregation at room temperature it is easy to handle while ensuring reliable results. Furthermore, **CoI2** is comparable in its aromatic scaffold to the co-initiator *p*-methylbenzylalcohol from our first study.[87] However, **CoI2** is a diol, which in theory allows the overall chain growth sites to be doubled as well.

For both co-initiators ROP of L-lactide was performed at different [LA]/[co-I]/[Cat]-ratios. Analog to our previous work, the [LA]/[Cat] ratios were chosen between 500:1 and 1500:1 with a common difference of 250. However, considering 1-hexanol (**CoI1**) is a liquid at room temperature, the Hamilton syringe causes a relatively large error if the sample volume of **CoI1**

Open Access Article. Published on 22 July 2025. Downloaded on 8/14/2025 4:27:06 AM.
This article is licensed under a Creative Commons Attribution 3.0 Unported Licence.

Faraday Discussions Accepted Manuscript

View Article Online
DOI: 10.1039/D5FD00062A

is small, such as at the ratio [LA]/[co-I]/[Cat] = 1500:1:1. Therefore, larger amounts of 3.31 *eq.*, 6.62 *eq.* as well as 10 *eq.* were used for the system with **CoI1**. In contrast, for simply weighed solid 1,4-benzenedimethanol (**CoI2**) the equivalence of 1 eq., 5 *eq.* and 10 *eq.* were used. Since **CoI2** contains two hydroxyl groups, which provide more reaction sites for lactide ROPs, the [LA]/[Cat]-ratios were increased to 2500:1, and the corresponding arithmetic difference was up to 500.

To evaluate the influence of **CoI1** and **CoI2** on the ROP, a characterization of the produced polymer by gel permeation chromatography was performed. The measured molar masses are compared with the corresponding theoretical molar masses (s. supporting information). **Table 1** summarizes the whole series of measurements with both co-initiator as well as without a co-initiator at a fixed [LA]/[Cat]-ratio of 500:1. As in our previous study, the concentration of polymer chains is calculated by the sum of co-initiator and catalyst loading. Consequently, the molar mass reduces with the increase of co-initiator, as more chain starters are contained in the polymerization mixture.[87] As mentioned above, different batches of L-lactide were used for each co-initiator, which causes a slight deviation due to varying water content. Considering the objective error, the series of measurements with **CoI1** is well matched, as the chains with M_n = 19700 g·mol^{-1} from polymerization with 3.31 eq **CoI1** were shorter than these without a co-initiator with M_n = 25700 g·mol^{-1}. Herein, the chains obtained from polymerization without a co-initiator were shorter than the theoretical one, probably due to the initiation of chain growth by the “asme”-ligand of **C1** and then decomposition of the catalyst.[74] Increasing the amount of **CoI1** to 6.62 eq and 10 eq yielded chains with 10500 g·mol^{-1} and 7800 g·mol^{-1}, respectively. For the case of **CoI2**, the chains with 40600 g·mol^{-1} from polymerization with 1 eq **CoI2** were longer than these without a co-initiator. The small amount of **CoI2** significantly accelerates the catalysis rate and also provides the possibility for the chain to grow in both sites simultaneously, and the conversion of L-lactide is higher, therefore the chain is longer than in the absence of a co-initiator. The molar mass of chains was decreased to 15900 g·mol^{-1} and 7700 g·mol^{-1} with an increase of **CoI2** to 5 eq and 10 eq. However, the experimental molar mass is not doubled as the theoretical molar mass, which indirectly illustrates that the activities of OH-groups at both sites of the diol might be different. When the amount of the diol is 10 eq, the result obtained is similar to the case of **CoI1**, which can be considered that the amount of **CoI2** approaches saturation. In addition, according to the deviation and the corresponding dispersity it can be considered that the chain growth could be controlled better with smaller deviation and dispersity in the presence of co-initiators compared to the case without a co-initiator. However, the effect of co-initiator does not improve linearly with the increasing loading.

Table 1: Comparison between experimental and theoretical molar masses of polymer obtained by L-lactide ROP at the [LA]/[Cat]-ratio of 500:1 with different co-initiators at different concentrations.

Co-I	eq	M_n [g·mol^{-1}] experimental	M_n [g·mol^{-1}] theoretical	deviation	mean	*Đ*
/	/	25700	42000	-39%	-46%	1.5
		19000	39300	-52%		1.7
1-hexanol (CoI1)	3.31	19700	13700	44%	60%	1.1
		23200	13200	76%		1.3
	6.62	10500	8500	24%	26%	1.1
		10800	8500	27%		1.1
	10	7800	6100	28%	30%	1.1
		8200	6200	32%		1.1
1,4-benzenedimethanol (CoI2)	1	40600	29400	38%	33%	1.4
		33400	26300	27%		1.5
	5	15900	11200	42%	42%	1.1
		16200	11400	42%		1.1
	10	7700	6300	22%	52%	1.1

Open Access Article. Published on 22 July 2025. Downloaded on 8/14/2025 4:27:06 AM.
This article is licensed under a Creative Commons Attribution 3.0 Unported Licence.

Faraday Discussions Accepted Manuscript

	11300	6200	82%	1.1

View Article Online
DOI: 10.1039/D5FD00062A

With these modified ratios mentioned above, the kinetic evaluation of lactide ROP was performed as described above. **Figure 1** presents the course of the semilogarithmic plot of conversion vs time for a [M]/[Co-I]/[Cat]-ratio of 500:10:1 for both **CoI1** and **CoI2**.

As described by equations 1-3, the slope of the semilogarithmic plot gives the apparent pseudo first order reaction rate constant k_{obs}. In comparison with our previous study, the curve behaviors of plot of conversion versus time are in good agreement.[87] For both **CoI1** as well as **CoI2** the apparent pseudo first order reaction rate constant k_{obs} decreased over reaction time. This is most likely caused by the single site catalytic behavior of **C1** with chain growth initiated by the "asme"-ligand.[74] This competes with the initiation by the external initiator and might cause a self-induced decomposition of the catalyst over the course of the polymerization. Therefore, model-based analysis is also helpful for these chosen co-initiators as will be discussed later.

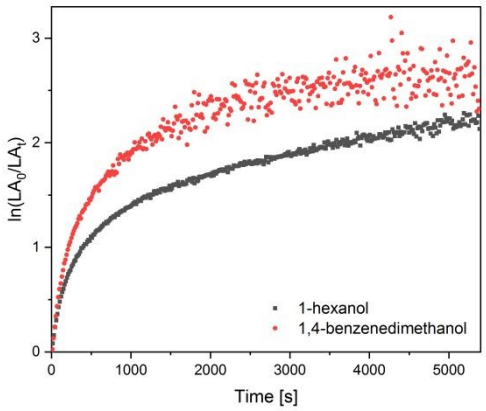

Figure 1: Semilogarithmic plot of conversion versus time of ROP of recrystallized L-lactide with **C1** and 1-hexanol (**CoI1**, black dots) and 1,4-benzenedimethanol (**CoI2**, red dots) at a [LA]/[co-I]/[Cat] ratio of 500:10:1 at 150 °C with a stirring speed 260 rpm and a reaction time of 90 min.

Nevertheless, herein classic kinetic analysis was performed also at various co-initiator loadings, which is normally not the case in literature due to the huge amount of necessary experimental work. Further, the obtained data will be used as the experimental supporting for the development of the analysis model. Due to the decrease of k_{obs} over time (**Figure 1**), only the initial range of the semilogarithmic plot, which shows a linear slope, was used to determine k_{obs} (**Figure 2**). Note, that due to the approximation the resulting data cannot be taken as absolute values. Therefore, the following kinetic discussion will focus on trends and given values should not be seen as absolute.

Open Access Article. Published on 22 July 2025. Downloaded on 8/14/2025 4:27:06 AM.
This article is licensed under a Creative Commons Attribution 3.0 Unported Licence.

Faraday Discussions Accepted Manuscript

View Article Online
DOI: 10.1039/D5FD00062A

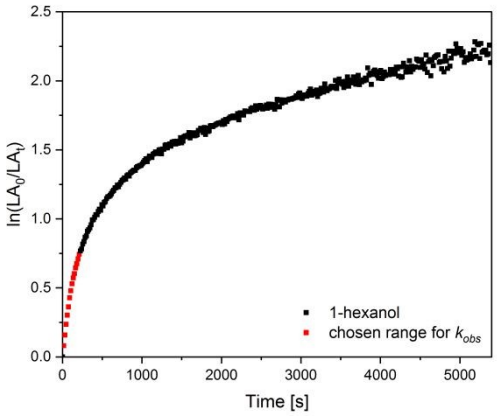

Figure 2: Semilogarithmic plot of conversion versus time of ROP of recrystallized L-lactide with **C1** and 1-hexanol (**Col1**) at a [LA]/[co-I]/[Cat] ratio of 500:10:1 at 150 °C with a stirring speed 260 rpm and a reaction time of 90 min.

Based on this principle k_{obs} was determined at different [LA]/[co-I]/[Cat]-ratios for both co-initiators. (s. Supporting information). As an example, the complete series of measurements with 10 eq. of 1-hexanol (**Col1**) is shown in **Figure 3**. In this case the polymerizations were carried out at [LA]/[Cat]-ratios between 500:1 and 1500:1.

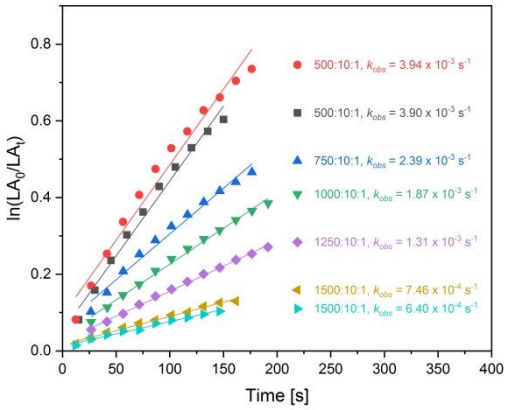

Figure 3: Semilogarithmic plot of conversion versus time of ROP of L-lactide with **C1** and 10 eq 1-hexanol (**Col1**) to determine the apparent rate coefficient k_{obs} from the initial range.

The determined k_{obs} values were used to determine the reaction rate constant k_p as the slope of a plot of k_{obs} versus concentration of catalyst **C1** for the different series of co-initiator loadings (**Table 2**). According to the results it can be seen, that an increase in co-initiator loading results in a higher k_p-value. This is due to the increased amounts of active sites for polymerization (OH-groups). Compared to *p*-methylbenzylalcohol (pMeBnOH) which was used previously, **Col2** containing a similar aromatic scaffold but twice the amount of OH-groups allows the catalysis rate to be doubled as well. As expected, the k_p = (11.9 ± 0.70) x 10^{-2} L mol^{-1} s^{-1} for **Col2** was determined, which is doubled as k_p = (5.03 ± 0.53) x 10^{-2} L mol^{-1} s^{-1} for pMeBnOH at the same conditions with 1 eq co-initiator (**Table 2**). Note that for each measurement series of co-initiators a different batch of lactide as well as **C1** was used, resulting in slight deviations due to varying water content in the monomer.

Table 2: Results of the kinetic evaluation of ROP of L-lactide with **C1** in the presence of different co-initiators

Co-Initiator	Equivalence	k_p x 10^{-2} [L mol^{-1} s^{-1}]

Open Access Article. Published on 22 July 2025. Downloaded on 8/14/2025 4:27:06 AM.
This article is licensed under a Creative Commons Attribution 3.0 Unported Licence.

Faraday Discussions Accepted Manuscript

/	/	3.43 ± 0.35
p-methylbenzylalcohol[89]	1	5.03 ± 0.53
	5	16.3 ± 1.8
	10	26.7 ± 2.8
1-hexanol (Col1)	3.31	14.9 ± 1.2
	6.62	19.1 ± 1.6
	10	28.7 ± 2.1
1,4-benzenedimethanol (Col2)	1	11.9 ± 0.70
	5	26.9 ± 0.60
	10	28.4 ± 1.7

View Article Online
DOI: 10.1039/D5FD00062A

Open Access Article. Published on 22 July 2025. Downloaded on 8/14/2025 4:27:06 AM.
This article is licensed under a Creative Commons Attribution 3.0 Unported Licence.

Although different the [LA]/[Cat]-ratios were used for **Col2** (500:1 to 2500:1 instead of 500:1 to 1500:1) when compared to **Col1** and pMeBnOH, the determined k_p in the presence of 10 eq of co-initiators are comparable within the scope of the error, for **Col1** k_p = (28.7 ± 2.1) x 10^{-2} L mol^{-1} s^{-1}, for pMeBnOH k_p = (26.7 ± 2.8) x 10^{-2} L mol^{-1} s^{-1} and for **Col2** k_p = (28.4 ± 1.7) x 10^{-2} L mol^{-1} s^{-1} were determined. Furthermore, the catalysis rate can be seen significantly enlarged in contrast to the k_p without co-initiator (**Figure 4**). However, in comparison to k_p-values from **Col1** and pMeBnOH with a used quantity of 10 eq, the corresponding k_p of CoI2 is similar even though **Col2** contains twice the amount OH-groups. This indicates that there is an upper limit to the rate increasing effect of a co-initiator. To visualize the contrast between **Col1** and **Col2**, the trend curve of k_p versus the added equivalents of the co-initiator is shown in **Figure 5 (left)**. As it can be seen, on the one hand the reaction rate accelerates linearly with an increasing amount of **Col1**. On the other hand, an even faster increase is observable if the loading of **Col2** is increased. However, an upper limit is clearly visible resulting in a saturation of the curve. Note, that 10 eq of **Col2** is equivalent to 20 eq of OH-groups initiating the chain growth. To eliminate the effect of the type of co-initiators on the reaction rate, the k_p values were plotted over the equivalents of OH-groups shown in **Figure 5 (right)**. The trend curves from both co-initiators show that an increase in the amount of OH-groups to 10 eq leads to a similar acceleration of reaction rate. Therefore, it can be considered that this is independent of the type of co-initiator. Moreover, the saturation is more clearly visible here, as is the huge added amount of OH-groups. It might be that the steric requirement for simultaneous polymerization of multiple sites is not necessarily given which might prevent the reaction rate from further increasing. This saturation was previously observed in the system that used $Sn(Oct)_2$ as a catalyst, the mono alcohol more than 20 eq used did not accelerate the reaction rate anymore.[92] Hence it might support that the limit of co-initiator is independent of the systems with different catalysts, rather dependent on the polymerization mechanism.

To verify this conjecture, the investigation of a precise mechanism in the presence of diol is necessary as well as the analysis of the influence of 20 eq of **Col1** on the reaction rate. However, classic kinetic analysis as presented above has critical limitations:

It requires high amounts of starting compounds needed lots of resources. This is in contrast to sustainable chemistry and therefore the overarching goals of the design of non-toxic ROP catalysts itself. Additionally, in the case of **C1** this approach by analyzing k_{obs} as well as k_p is not an absolute method but rather an approximation. Since the validity range of the determination of k_{obs} is approximated the method depends strongly on the experimental conditions and resulting data. [73] Therefore, the development of a model-based analysis is necessary for giving a more reliable, unbiased and resource-efficient way to evaluate the performance of these co-initiators for lactide ROP.

Faraday Discussions Accepted Manuscript

View Article Online
DOI: 10.1039/D5FD00062A

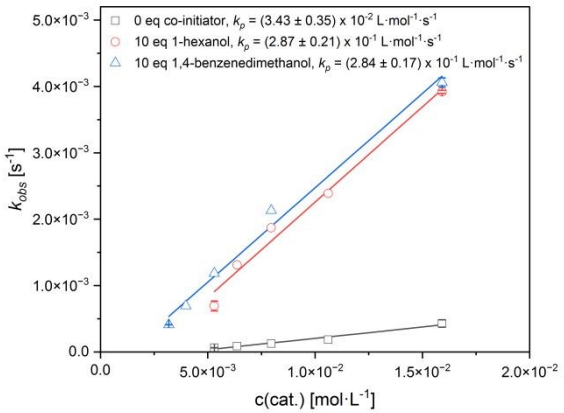

Figure 4: Determination of the reaction rate constant k_p of ROP of L-lactide with **C1** and 10 eq 1-hexanol (**Col1**, red dots) and 1,4-benzenedimethanol (**Col2**, blue dots), or without co-initiator (black dots) by plotting the apparent rate coefficient k_{obs} from the initial ranges over the catalyst concentration.

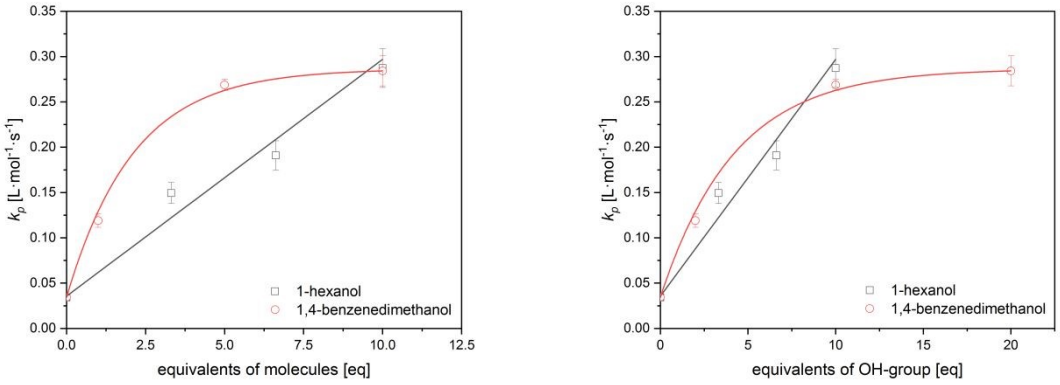

Figure 5: Plot of the reaction rate constant from the slopes of the initial range versus the loading of different co-initiators (left) or the equivalents of OH-groups (right).

Development of a kinetic model for ROP with different co-initiators

The analysis of the experimental data described so far enables a direct comparison of the activity of different catalyst/co-I systems but is not sufficient for prediction of the time course of monomer conversion or prediction of the molar mass distribution. These two key figures are essential for setting optimum operating points in an industrial application. Furthermore, the underlying chemical relationships are to be investigated in greater depth to enable the development of improved catalyst co-initiator systems. For this purpose, a kinetic model is proposed that includes the relevant reactions. As described above, ROP of lactide with the catalyst takes place according to a coordination-insertion mechanism and the ligand of the catalyst can also acts as a chain initiator and the catalytically active centre splits off in the process.[74,87] It has already been shown in the literature that zinc alcoholates are also active in the ROP.[90] However, this activity is significantly lower than for the catalyst, which explains why the apparent reaction rate decreases significantly as the reaction progresses.

Based on this finding, the model previously developed by the authors is extended in this work to include the catalytic activity of the metal species formed after the split-off of the catalyst metal centre.[87] Note, that due to the reaction conditions a clear specification of this less active species is not possible. Since both, $ZnCl_2$ and Zn alkoxide might act as weak catalyst a further

Open Access Article. Published on 22 July 2025. Downloaded on 8/14/2025 4:27:06 AM.
This article is licensed under a Creative Commons Attribution 3.0 Unported Licence.

Faraday Discussions Accepted Manuscript

specification of the active species is not made. **Scheme 2** is set up to model the reaction system of the use of mono-functional co-initiators:

View Article Online
DOI: 10.1039/D5FD00062A

(a) Catalyst activation

$$D_n + C \underset{k_{C,a2}}{\overset{k_{C,a1}}{\rightleftharpoons}} R_{C,n} + A_C$$

$$D_n + CR \underset{k_{CR,a2}}{\overset{k_{CR,a1}}{\rightleftharpoons}} R_{CR,n} + A_{CR}$$

(b) Chain initiation

$$C + M \xrightarrow{k_{CM}} D_2 + CR$$

(c) Propagation

$$R_{i,n} + M \underset{k_{i,d}}{\overset{k_{i,p}}{\rightleftharpoons}} R_{i,n+2}$$

(d) Chain transfer

$$R_{i,n} + R_{j,k} \underset{k_s}{\overset{k_s}{\rightleftharpoons}} R_{i,k} + R_{j,n}$$

$$R_{i,n} + D_k \underset{k_s}{\overset{k_s}{\rightleftharpoons}} R_{i,k} + D_n$$

(e) Intermolecular transesterification

$$R_{i,n} + D_k \underset{k_{tr}}{\overset{k_{tr}}{\rightleftharpoons}} R_{i,n+k-p} + D_p$$

$$R_{i,n} + G_k \underset{k_{tr}}{\overset{k_{tr}}{\rightleftharpoons}} R_{i,n+k-p} + G_p$$

(f) Random chain scission

$$R_{i,n} \xrightarrow{k_{de}} R_{i,n-k} + G_k$$

$$D_{i,n} \xrightarrow{k_{de}} D_{i,n-k} + G_k$$

$$G_{i,n} \xrightarrow{k_{de}} G_{i,n-k} + G_k$$

Small molecules:

- C: Catalyst
- CR: Catalyst residue
- M: Monomer
- A_C: Byproduct from catalyst activation
- A_{CR}: Byproduct from catalyst residue activation
- $R_{i,j,0}$: Initiator
- D_0: Alcohol co-initiator

Macromolecules:

- R: Active (reactive) chain
- D: Inactive (dormant) chain
- G: Terminated chain

Indices:

- i: chain end, $\in [C; CR]$
- n, k, p: chain length, $\in [0 \quad \infty]$

Scheme 2*:* Proposed scheme for the summarised kinetics for ROP of lactide with "asme" type catalyst and a monofunctional alcohol as co-initiator.

The nomenclature of the polymer species is based on literature in this field for the $Sn(Oct)_2$ catalyzed ROP.[91–97] Polymer chains are divided into active (R), inactive (D) and terminated (G) populations. The active chains are divided into chains with a catalyst (C) and chains with a catalyst rest (CR) at the end of the chain. The index of the populations represents the number of repeating units. The lactoyl unit is chosen to enable a more accurate description of transesterification reactions.

Reactions (a) describe the activation of co-initiator (for n = 0) or an inactive chain (for n > 0) with catalyst or catalyst residue forming an initiator (n = 0) or an active chain (n > 0) with catalyst or catalyst residue as a chain end. This activation is an equilibrium reaction with equilibrium constant $K_{\mathrm{eq,a}} = k_{\mathrm{a1}}/k_{\mathrm{a2}}$. The activation is assumed much faster than the chain propagation and is therefore modelled as quasi-instantaneous. This is in accordance with studies for $Sn(Oct)_2$ as catalyst and can be seen for the “asme” type catalysts as well since no induction period is visible after melting of lactide.

Reaction (b) means that, in addition to the activated co-initiator, the ligand of the catalyst can also act as a chain initiator with reaction rate constant k_{CM}. The reaction with a monomer produces an inactive chain with two repeating units with the elimination of a catalyst residue.

Reaction (c) describes the actual propagation of an active chain by reaction with a monomer to form an active chain that is two repeating units longer with the reaction constants $k_{\mathrm{C,p}}$ for catalyst at the chain end and $k_{\mathrm{CR,p}}$ for catalyst residue at the chain end. The reaction is assumed to be an equilibrium reaction. The equilibrium constant can be calculated from the maximum achievable conversion. For $n = 0$ an initiator molecule starts an active chain with two repeating units.

Open Access Article. Published on 22 July 2025. Downloaded on 8/14/2025 4:27:06 AM.
This article is licensed under a Creative Commons Attribution 3.0 Unported Licence.

Faraday Discussions Accepted Manuscript

View Article Online
DOI: 10.1039/D5FD00062A

Reaction (d) describes the chain transfer. This consists of the exchange of active chain ends between active and inactive chains. This reaction has no influence on the monomer conversion but is essential for mapping the molecular mass distribution. Due to the equivalence of forward and reverse reactions, an equilibrium constant of one is assumed.[92]

Reactions (e) describe intermolecular transesterification reactions with the reaction rate constant k_{te}. These significantly influence the width of the molecular mass distribution. Analogous to the chain transfer reactions, an equilibrium constant of one is assumed here due to the equivalence of the forward and reverse reactions.

Random chain scission reactions are represented by the reactions (f). Polymer chains irreversibly break into terminated chains at a random point with the reaction rate constant k_{de}. This reaction is only relevant at elevated temperatures with high thermal stress.

In contrast to the use of a monoalcohol like **ColI**, there are two activation stages when using a diol as a co-initiator, which are depicted in **Scheme 3**. The result of the second stage corresponds to the PLA shown in **Scheme 1.**

$$\begin{aligned}
&\text{1. activation stage} && \mathrm{HO{-}R{-}OH + ZnL_n \rightleftharpoons HO{-}R{-}O{-}ZnL_{n-1} + A}\\
&\text{2. activation stage} && \mathrm{HO{-}R{-}O{-}ZnL_{n-1} + ZnL_n \rightleftharpoons L_{n-1}Zn{-}O{-}R{-}O{-}ZnL_{n-1} + A}
\end{aligned}$$

Scheme 3: Reaction equations for two-stage catalyst (ZnL_n) activation with a bi-functional co-initiator.

Both OH groups of the co-initiator can form an active species by ligand exchange with the ligand of the catalyst, splitting off an acid residue. This also leads to polymer chains that can have two active chain ends. Overall, this results in the following more complex reaction network depicted in **Scheme 4.**

Open Access Article. Published on 22 July 2025. Downloaded on 8/14/2025 4:27:06 AM.
This article is licensed under a Creative Commons Attribution 3.0 Unported Licence.

Faraday Discussions Accepted Manuscript

View Article Online
DOI: 10.1039/D5FD00062A

Open Access Article. Published on 22 July 2025. Downloaded on 8/14/2025 4:27:06 AM.
This article is licensed under a Creative Commons Attribution 3.0 Unported Licence.

Faraday Discussions Accepted Manuscript

(a) 1. catalyst activation

$$D_n + C \underset{k_{C,a2}}{\overset{2\ k_{C,a1}}{\rightleftharpoons}} R_{C,n} + A_C$$

$$D_n + CR \underset{k_{CR,a2}}{\overset{2\ k_{CR,a1}}{\rightleftharpoons}} R_{CR,n} + A_{CR}$$

2. catalyst activation

$$R_{i,n} + C \underset{2\ k_{C,a2}}{\overset{k_{C,a1}}{\rightleftharpoons}} R_{i,C,n} + A_C$$

$$R_{i,n} + CR \underset{2\ k_{CR,a2}}{\overset{k_{CR,a1}}{\rightleftharpoons}} R_{i,CR,n} + A_{CR}$$

(b) Chain initiation

$$C + M \xrightarrow{k_{CM}} D_2 + CR$$

(c) Propagation

$$R_{i,n} + M \underset{k_{i,d}}{\overset{k_{i,p}}{\rightleftharpoons}} R_{i,n+2}$$

$$R_{i,i,n} + M \underset{2\ k_{i,d}}{\overset{2\ k_{i,p}}{\rightleftharpoons}} R_{i,i,n+2}$$

$$R_{C,CR,n} + M \underset{k_{C,d}}{\overset{k_{C,p}}{\rightleftharpoons}} R_{C,CR,n+2}$$

$$R_{C,CR,n} + M \underset{k_{CR,d}}{\overset{k_{CR,p}}{\rightleftharpoons}} R_{C,CR,n+2}$$

(d) Chain transfer

$$R_{i,j,n} + D_k \underset{k_s}{\overset{k_s}{\rightleftharpoons}} R_{i,j,k} + D_n$$

$$R_{i,j,n} + D_k \underset{k_s}{\overset{k_s}{\rightleftharpoons}} R_{i,k} + R_{j,n}$$

$$R_{i,j,n} + R_{i,k} \underset{k_s}{\overset{k_s}{\rightleftharpoons}} R_{i,j,k} + R_{i,n}$$

$$R_{i,n} + R_{j,k} \underset{k_s}{\overset{k_s}{\rightleftharpoons}} R_{i,k} + R_{j,n}$$

$$R_{i,n} + D_k \underset{k_s}{\overset{k_s}{\rightleftharpoons}} R_{i,k} + D_n$$

(e) Intermolecular transesterification

$$R_{i,j,n} + R_{i,j,k} \underset{k_{tr}}{\overset{k_{tr}}{\rightleftharpoons}} R_{i,j,n+k-p} + R_{i,j,p}$$

$$R_{i,j,n} + R_{i,k} \underset{k_{tr}}{\overset{k_{tr}}{\rightleftharpoons}} R_{i,j,n+k-p} + R_{i,p}$$

$$R_{i,j,n} + D_k \underset{k_{tr}}{\overset{k_{tr}}{\rightleftharpoons}} R_{i,j,n+k-p} + D_p$$

$$R_{i,j,n} + G_k \underset{k_{tr}}{\overset{k_{tr}}{\rightleftharpoons}} R_{i,j,n+k-p} + G_p$$

$$R_{i,n} + D_k \underset{k_{tr}}{\overset{k_{tr}}{\rightleftharpoons}} R_{i,n+k-p} + D_p$$

$$R_{i,n} + G_k \underset{k_{tr}}{\overset{k_{tr}}{\rightleftharpoons}} R_{i,n+k-p} + G_p$$

(f) Random chain scission

$$R_{i,j,n} \xrightarrow{k_{de}} R_{i,j,n-k} + G_k$$

$$R_{i,n} \xrightarrow{k_{de}} R_{i,n-k} + G_k$$

$$D_{i,n} \xrightarrow{k_{de}} D_{i,n-k} + G_k$$

$$G_{i,n} \xrightarrow{k_{de}} G_{i,n-k} + G_k$$

Small molecules:

- C: Catalyst
- CR: Catalyst residue
- M: Monomer
- A_C: Byproduct from catalyst activation
- A_{CR}: Byproduct from catalyst residue activation
- $R_{i,j,0}$: Initiator
- D_0: Alcohol co-initiator

Macromolecules:

- R: Active (reactive) chain
- D: Inactive (dormant) chain
- G: Terminated chain

Indices:

- i, j: chain end, $\in [C; CR]$
- n, k, p: chain length, $\in [0 \quad \infty]$

Scheme 4: Proposed scheme for the summarised kinetics for the ROP of lactide with "asme" type catalyst and bi-functional alcohol as co-initiator.

The reactions now include a second activation step, during which a ligand exchange occurs between the second hydroxyl group of the co-initiator and the catalyst or catalyst residue. It is important to note that the relevant factor for determining reaction rates is not the concentration of active or inactive chains, but rather the concentration of active or inactive chain ends. This is reflected in the reaction scheme by incorporating a factor of 2 into the reaction rate constant for the forward reaction of the first stage and the reverse reaction of the second stage. Furthermore, active chains must be distinguished not only based on their active end but also according to the number of active ends present. In the scheme provided, this differentiation is

View Article Online
DOI:10.1039/D5FD00062A

achieved using the indices i and j, which represent either a catalyst-bound chain end or a chain end associated with a catalyst residue. This distinction introduces a significant number of additional reactions, including propagation, chain transfer, intermolecular transesterification, and random chain scission, all of which must be accounted for to achieve accurate modeling.

Mathematical description of the reaction systems

The component mass balances for the small molecules and population balances for the polymer species for a batch reactor are drawn up for both reaction systems, assuming an isochoric reaction.[98] This assumption is justified because of the only small differences in density between lactide and PLA. The resulting system of partial differential equations is converted into a system of ordinary differential equations using the method of moments. As suggested in literature the specific chain lengths R_1 and R_0 are omitted in the final equations.[91–93] Solving the equation system one can calculate chain properties including conversion X, number average molecular mass M_n and dispersity Đ. The moments of the polymer populations are defined due to the following equation:

$$\mu_i^P = \sum_{n=0}^{\infty} n^i P_n \qquad (P = R_{C,C}, R_{C,CR}, R_{CR,CR}, R_C, R_{CR}, D, G) \tag{4}$$

In this equation P symbolyzes any occuring polymeric species, n is the number of repeating units and i the order of the moment.

The moments 0 to 3 are used for the mathematical description of the system. A gamma distribution is assumed for the chain length distribution. The following relationship can be derived as the closing condition for the calculation of the 3rd moment:[99]

$$\mu_3^P = \frac{\mu_2^P\left(2\,\mu_2^P\mu_0^P - \left(\mu_1^P\right)^2\right)}{\mu_1^P\mu_0^P} \tag{5}$$

The complete differential equation system of both reaction systems including all mass balances, population balances and moment equations can be found in the supporting information. For the general derivation of moment equations, please refer to the literature.[100,101]

X, M_n and Đ are then calculated using the following equations:

$$X = \frac{M_0 - M}{M_0} \tag{6}$$

$$r_n = \frac{\sum_P \mu_1^P}{\sum_P \mu_0^P} \tag{7}$$

$$M_n = r_n m_{\mathrm{Mon}} + m_{\mathrm{I}} \tag{8}$$

$$r_w = \frac{\sum_P \mu_2^P}{\sum_P \mu_1^P} \tag{9}$$

$$Đ = \frac{r_{\mathrm{w}}}{r_{\mathrm{n}}} \tag{10}$$

Here, r_n and r_w represent number and weight average chain length. Note that m_{Mon} is the molar mass of the lactoyl repeating unit. m_{I} denotes the molecular mass of the initiator species that is formed in the activation step from reaction of catalyst and co-initiator.

Parameter estimation

Open Access Article. Published on 22 July 2025. Downloaded on 8/14/2025 4:27:06 AM.
This article is licensed under a Creative Commons Attribution 3.0 Unported Licence.

Faraday Discussions Accepted Manuscript

View Article Online
DOI: 10.1039/D5FD00062A

Open Access Article. Published on 22 July 2025. Downloaded on 8/14/2025 4:27:06 AM.
This article is licensed under a Creative Commons Attribution 3.0 Unported Licence.

Faraday Discussions Accepted Manuscript

The reaction system described requires the determination of seven unknown reaction parameters that cannot be determined from literature. To minimize parameter correlation, determination proceeds in a sequential manner through four distinct steps. During all these steps, deviations between experimental data and model data are minimized with a least squares objective function.

Step 1: Experiments utilizing $ZnCl_2$ as catalyst are employed to determine the reaction parameters for activation and propagation with catalyst residues ($k_{\mathrm{CR,p}}, K_{\mathrm{CR,A}}$).

Step 2: A reduced reaction system is utilized to determine the propagation and activation parameters of the ROP with catalyst ($k_{\mathrm{CM}}, k_{\mathrm{C,p}}, K_{\mathrm{C,A}}$). Equations (d) through (f) can be disregarded in this step, as they exert no influence on monomer concentration but merely broaden or shift the molecular mass distribution.

Step 3: The system from step 2 together with reactions (f) are used to determine the kinetic parameter of random chain scission k_{de} by minimizing deviations in the number average molecular mass of the polymer. Intermolecular transesterification reactions can be neglected since they only contribute to symmetrically broadening the molecular mass distribution and therefore do not influence the number average molecular mass.

Step 4: The complete kinetic scheme is used to determine the kinetic parameter of the intermolecular transesterification reaction k_{te} by minimizing deviations in the dispersity of the molecular mass distribution of the polymer.

To enhance parameter identifiability and comparability, it is postulated that chain initiation by the ligand occurs independently of the co-I employed. Consequently, k_{CM} is determined exclusively for *p*-MeBnOH and maintained constant for the other two co-I. Furthermore, it is assumed that transesterification and chain scission have the same rate constant for all polymer populations.

The systems of differential equations are solved in MATLAB using the *ode15s* solver. Parameter estimations were performed minimizing the respective objective function in MATLAB using built-in *lsqnonlin* function.

Results of the parameter estimation

The resulting kinetic parameters from the parameter estimation for the $ZnCl_2$ catalysed reaction are presented in **Table 3**. As only one experiment (see Table S1) was used for parameterisation and the two parameters are strongly correlated, the confidence intervals are comparatively wide. These were assumed to be sufficiently accurate for this work, as the activity of the deteriorated catalyst part is significantly lower than that of the catalyst. Accordingly, this influence is less relevant. In line with this reasoning, the rate constants for $ZnCl_2$ catalysed ROP with the two other co-I used in this work were not determined.

Table 3: Fitted parameter set according to step 1 for $ZnCl_2$ as catalyst for the polymerization of l-lactide at 150 °C with 95 % confidence intervals.

Parameter	Unit	Value	Lower bound	Upper bound
$k_{\mathrm{CR,p}}$	L mol^{-1} s^{-1}	0.0032	0.0014	0.0052
$K_{\mathrm{CR},a}$	-	0.0471	-0.0109	0.0949

An overview of all experiments conducted in this work and used for parameterisation and further analysis are shown in **Table S3-S5** (for CoI1) and **Table S6-S8** (for CoI2). Further experiments used for parameterisation and analysis of *p*-MeBnOH are taken from Conen et al. and Fuchs.[87,89] **Table 4** lists the kinetic parameters determined according to step 2 for all co-I

View Article Online
DOI: 10.1039/D5FD00062A

tested. In addition, the 95% confidence intervals of the parameter estimates are given to categorise the reliability. Firstly, it can be noted that the values for the propagation rate constant $k_{\mathrm{C,p}}$ are of a similar order of magnitude for all co-I. The equilibrium constant of the catalyst activation $K_{C,a}$ is also very similar for **CoI1** and *p*-MeBnOH, but the value for the **CoI2** is significantly higher. The confidence intervals are very narrow for all parameters, which indicates a high precision of the parameters for the experimental data used.

Table 4: Fitted parameter set according to step 2 for the polymerization of l-lactide with catalyst at 150 °C with 95 % confidence intervals for both co-I tested and *p*-MeBnOH[87,89].

Co-Initiator	Parameter	Unit	Value	Lower bound	Upper bound
p-MeBnOH	k_{CM}	s^{-1}	581.4	530.9	631.8
	$k_{\mathrm{C,p}}$	$\mathrm{L\ mol^{-1}\ s^{-1}}$	1.304	1.214	1.394
	$K_{C,a}$	-	2460	2314	2606
CoI1	$k_{\mathrm{C,p}}$	$\mathrm{L\ mol^{-1}\ s^{-1}}$	1.185	1.169	1.201
	$K_{C,a}$	-	3362	3305	3419
CoI2	$k_{\mathrm{C,p}}$	$\mathrm{L\ mol^{-1}\ s^{-1}}$	1.079	1.049	1.109
	$K_{C,a}$	-	29,630	28,511	30,750

The mean absolute errors for the parametrisations regarding the conversion are listed in **Table 5**.

Table 5: Mean absolute errors of conversion for the parametersations of all co-I tested and *p*-MeBnOH[87,89].

Co-Initiator	MAE for conversion
p-MeBnOH	0.039
CoI1	0.057
CoI2	0.056

For all co-I, the MAE is less than 6%, which indicates an acceptable agreement between experimental data and model. For p-MeBnOH as a co-I, this deviation is even less than 4%. A possible explanation for this, in addition to deviations in the accuracy of experimental data, lies in the procedure used. Since, in contrast to the two other co-Is, the value for k_{CM} was also released as a fit parameter, a more precise adjustment to the experimental data used is possible here due to the model.

The parameters k_{te} and k_{de} relevant for the model-based description of the molecular mass distribution are listed in

Table 6 together with the 95% confidence intervals. These parameters were determined using the methodology described in steps 3 and 4. Again, only minor deviations between experimental data and model prediction are recognisable for the dispersity of the molecular mass distribution. The parameters determined for k_{te} are of a similar order of magnitude for all co-Is tested and match findings reported for $Sn(Oct)_2$ as catalyst.[92,93] For all experiments used for parameterisation, the measured dispersities range between 1.05 and 1.3. On one hand, this reduces the reliability of k_{te} for areas with higher dispersities. On the other hand, this demonstrates that with the catalyst co-initiator systems used, the dispersities are in low ranges and therefore the breadth of the distribution for these systems is not particularly problematic.

Open Access Article. Published on 22 July 2025. Downloaded on 8/14/2025 4:27:06 AM.
This article is licensed under a Creative Commons Attribution 3.0 Unported Licence.

Faraday Discussions Accepted Manuscript

View Article Online
DOI: 10.1039/D5FD00062A

For the simulative description of the number-average molar mass, on the other hand, there are larger deviations. For **CoI1**, even the determined value for k_{de} becomes 0, since a large part of the measured mean molar masses are already higher than the simulatively calculated ones for $k_{\mathrm{de}} = 0$. The uncertainty regarding the parameter estimation is already clear when looking at the confidence intervals, as these contain 0 for all co-Is. However, this is also consistent with literature data that at 150 °C k_{de} assumes low values due to the still comparatively low thermal load[93,95] or is even completely neglected in most publications.[91,92,96] Another factor that may play a role in this phenomenon is the initiation efficiency, as this leads to longer chain lengths than predicted by the model.

Table 6: Fitted parameter set according to step 3 and 4 for the polymerization of l-lactide with catalyst at 150 °C with 95 % confidence intervals for all co-I tested and *p*-MeBnOH[87,89].

Co-Initiator	Parameter	Unit	Value	Lower bound	Upper bound
p-MeBnOH	k_{te}	s^{-1}	0.00118	-0.00572	0.00808
	k_{de}	$\mathrm{L\ mol^{-1}\ s^{-1}}$	3.99×10^{-7}	-2.37×10^{-6}	3.17×10^{-6}
CoI1	k_{te}	s^{-1}	0.00178	-0.01172	0.01529
	k_{de}	$\mathrm{L\ mol^{-1}\ s^{-1}}$	0	-	-
CoI2	k_{te}	s^{-1}	0.00228	-0.0272	0.0317
	k_{de}	$\mathrm{L\ mol^{-1}\ s^{-1}}$	8.00×10^{-9}	-1.69×10^{-8}	3.29×10^{-8}

Table 7 lists the mean absolute errors of the parameter estimations for number average molecular mass and dispersity of the molecular mass distribution. As already described, there are sometimes high deviations between the model and experimental data, which is why there are comparatively high deviations in the M_n. The errors in dispersity, on the other hand, are significantly lower.

Table 7*:* Mean absolute errors for the estimation of transesterification and chain scission parameters according to steps three and four for all co-Is.

Co-Initiator	MAE for M_n in $\frac{\mathrm{g}}{\mathrm{mol}}$	MAE for Đ
p-MeBnOH	5126	0.0365
CoI1	12649	0.0871
CoI2	6480	0.0648

In order to gain an initial insight into the suitability of the underlying reaction system for modelling the ROP, the reaction parameters determined from the experiments with co-I are used for extrapolation to experiments without co-I. Here, the influence of the chain start by catalyst is much more pronounced, as this must inevitably take place in order for polymer chains to be formed, which can then grow. Accordingly, this property of the catalysts used must be accurately described for good predictions of the polymerisation process. In addition to the comparison of modelling and experimental data, the internal consistency between the modelling of mono-functional and bi-functional co-Is can also be tested here. For a co-I concentration of 0, both model parameterisations for a mono-functional alcohols as co-I and the model for a bi-functional alcohols as co-I should produce an equal conversion curve. **Figure** shows this comparison together with experimental data for a [LA]/[Cat] ratio of 500:1. There is very little deviation for the two mono-functional co-I models. For the bi-functional co-I model, slight deviations can be recognised both qualitatively and quantitatively, but these are within an acceptable range overall. All models show satisfactory results, especially when compared with experimental data.

Open Access Article. Published on 22 July 2025. Downloaded on 8/14/2025 4:27:06 AM.
This article is licensed under a Creative Commons Attribution 3.0 Unported Licence.

Faraday Discussions Accepted Manuscript

View Article Online
DOI: 10.1039/D5FD00062A

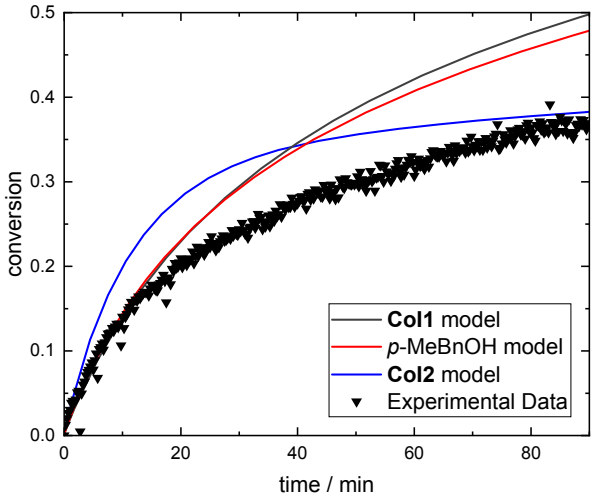

Figure 6*:* Comparison of model for all three co-I parameterisations and experimental data for monomer conversion over time for a ratio [LA.]/[co-I]/[Cat] of 500/0/1.

Figure 7also shows the comparison of models with experimental data for reaction systems without co-I. In panel (a), the conversion profiles are plotted against the ratio of initial monomer to catalyst concentration ([LA]/[Cat]). Here, the different models should produce identical curve progressions, which is observable with only minor deviations. The comparison with experimental data demonstrates that the extrapolation capability of the models yields acceptable results even outside the concentration ranges used for parameterisation.

Panel (b) shows the same comparison for the dispersity of the molecular mass distribution. The absence of co-initiator leads to a loss of the controllability over the reaction which can be seen at the significantly higher dispersities even at lower conversions. Here, the extrapolation capability of the model is significantly more challenging, as the experiments used for parameterisation all had dispersities in the range of 1.05 to 1.3, which is considerably lower than the measured dispersities of 1.4 to 1.8 for experiments without co-I. The experimental results are quantitatively matched much less accurately than for the conversion. Nevertheless, it is qualitatively observable that all models predict significantly higher dispersities for initial formulations without co-I compared to experiments with co-I, suggesting that the underlying chemical mechanisms are represented qualitatively.

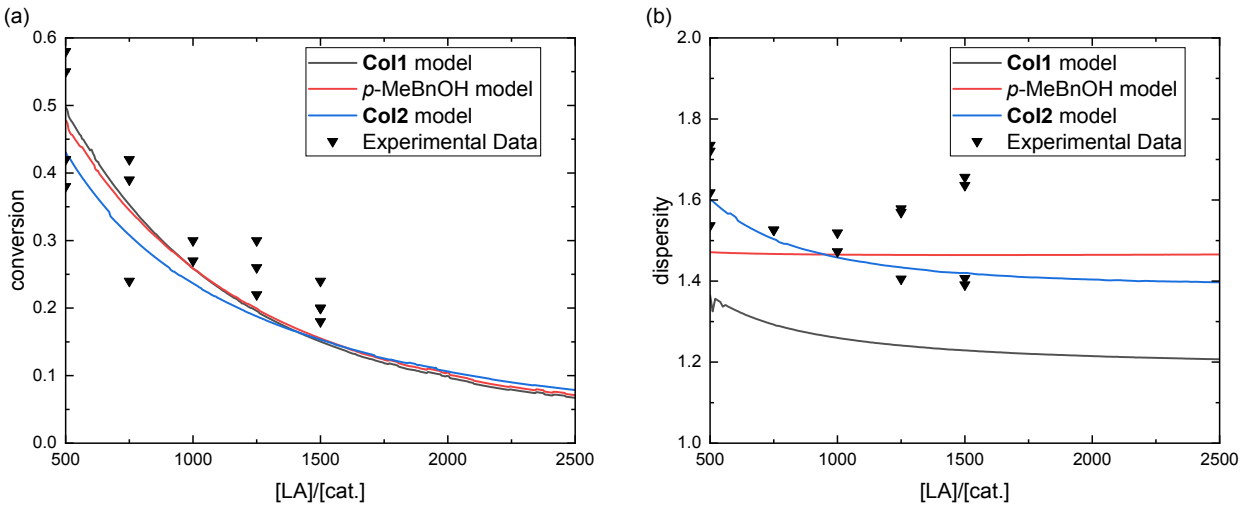

Open Access Article. Published on 22 July 2025. Downloaded on 8/14/2025 4:27:06 AM.
This article is licensed under a Creative Commons Attribution 3.0 Unported Licence.

Faraday Discussions Accepted Manuscript

View Article Online
DOI: 10.1039/D5FD00062A

Figure 7: Comparison of experimental data and model predictions for experiments without co-I over ratio monomer to catalyst concentration for (a) conversion and (b) dispersity after 90 minutes reaction time. Experimental data for *p*-MeBnOH are taken from Conen et al.[87] and Fuchs[89].

Model based analysis of the co-initiator influence

Based on the determined kinetic parameters, it can already be concluded that the use of **CoI1** or p-MeBnOH only leads to minor differences in the measured conversion and thus also in the suitability for catalyst activation. For the use of **CoI2**, a significant difference to the two previous co-Is can already be determined based on the equilibrium of the catalyst activation. The value of the equilibrium constant of the activation $K_{C,a}$ is significantly higher, whereby considerable advantages in achieving high conversions can be determined, particularly with the "asme" type catalyst used. The high equilibrium constant has two effects that both increase the conversion. These can be illustrated using the reaction equations (a) and (b) of the reaction system in **Scheme 2**. As already described, the catalyst activation in equation (a) is assumed to be quasi-instantaneous, i.e. this reaction is always in equilibrium. The equilibrium of the reaction can be described using the equilibrium constant $K_{C,a}$ as follows:

$$K_{C,a} = \frac{\mu_0^{R_C} \times A_C}{C \times \mu_0^D} \tag{11}$$

On the one side increasing the equilibrium constant increases the concentration of active polymer chains $\mu_0^{R_C}$ that can propagate. On the other side it reduces the concentration of unbound catalyst C, which in turn leads to a reduced reaction rate of the chain start by catalyst even at the same value for k_{CM}. The second effect in particular leads to a significant improvement in the potential of "asme" type catalysts for industrial ROP. Both effects can be seen in **Figure 8** for an initial ratio of [LA]/[co-I]/[Cat] of 500:5:1. The conversion for the bi-functional co-I increases significantly faster and reaches a higher final value after 90 minutes (a). The two mono-functional co-Is show only minor differences. In (b), it is evident that the ratio of polymer chains with catalyst at the end to initially used catalyst for the bi-functional co-I is considerably higher from the beginning compared to the mono-functional co-Is. This is derived from the first mentioned effect. Additionally, it is noticeable that this ratio decreases more slowly, which can be attributed to the slower chain initiation by the catalyst.

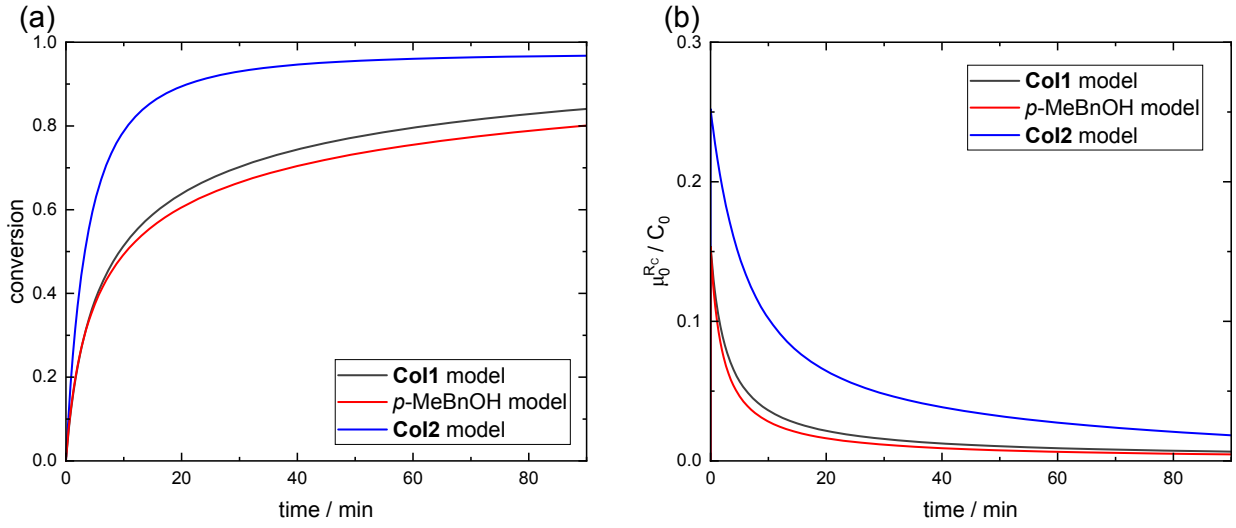

Figure 8: Effects of higher activation equilibrium constants on (a) conversion and (b) ratio of active chains with catalyst end to initial catalyst concentration over time for 90 minutes.

The influence of co-I concentration for all tested co-Is on the conversion after 90 minutes of reaction time is shown in **Figure 9**. Overall, acceptable agreements between experimental

Open Access Article. Published on 22 July 2025. Downloaded on 8/14/2025 4:27:06 AM.
This article is licensed under a Creative Commons Attribution 3.0 Unported Licence.

Faraday Discussions Accepted Manuscript

View Article Online
DOI: 10.1039/D5FD00062A

data and model predictions are observable. All models predict similar values for the reaction system without co-I. However, with increasing co-I concentration, the predicted conversions for the bi-functional co-I increase significantly more and reach the equilibrium conversion of the polymerization already at 5 co-I equivalents. For the two mono-functional co-Is, this would only be achieved at about 25 co-I equivalent. The decisive factors for this effect are again the previously described effects due to the increased equilibrium constant of catalyst activation.

It is noteworthy that for co-I ratios of [co-I]/[Cat] < 1, no advantage of the bi-functional co-I is apparent but further increasing co-I concentrations leads to more strongly increasing conversions. A possible explanation for this is that the equilibrium of activation is not determined by the co-I concentration, but by the concentration of OH groups, and this increases twice as fast for the bi-functional co-I as for the mono-functional co-Is with increasing co-I concentration.

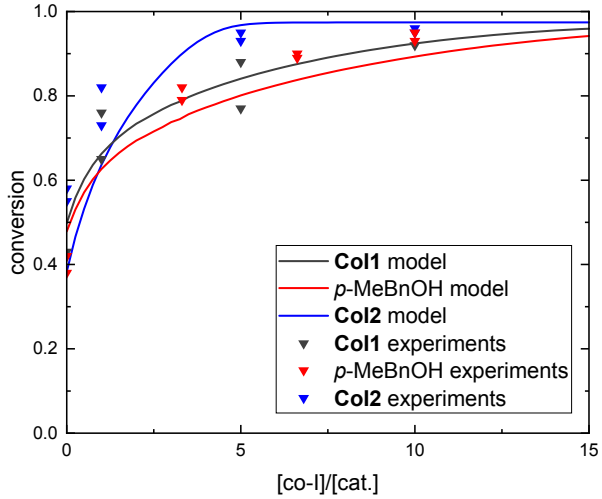

Figure 9: Influence of co-initiator concentration (as ratio of co-I to catalyst) for fixed monomer to catalyst ratio [LA]/[Cat] = 500/1 on conversion after 90 minutes reaction time. Experimental data for *p*-MeBnOH are taken from Conen et al.[87] and Fuchs[89].

In this context, it is also interesting to plot the conversion against the catalyst concentration at a constant co-I concentration (see **Figure 10**). Here it can again be seen that only small differences occur for the two mono-functional co-Is. For the bifunctional co-I, on the other hand, the conversions achieved are significantly higher. However, the deviation decreases significantly for lower catalyst concentrations. This can be explained by the fact that for low catalyst concentrations at higher co-I concentrations, the influence of the chain start by catalyst is greater and therefore the influence of catalysis by catalyst residue is higher. Accordingly, the achievable conversions are generally lower, as is the difference between mono- and bifunctional co-Is.

Open Access Article. Published on 22 July 2025. Downloaded on 8/14/2025 4:27:06 AM.
This article is licensed under a Creative Commons Attribution 3.0 Unported Licence.

Faraday Discussions Accepted Manuscript

View Article Online
DOI: 10.1039/D5FD00062A

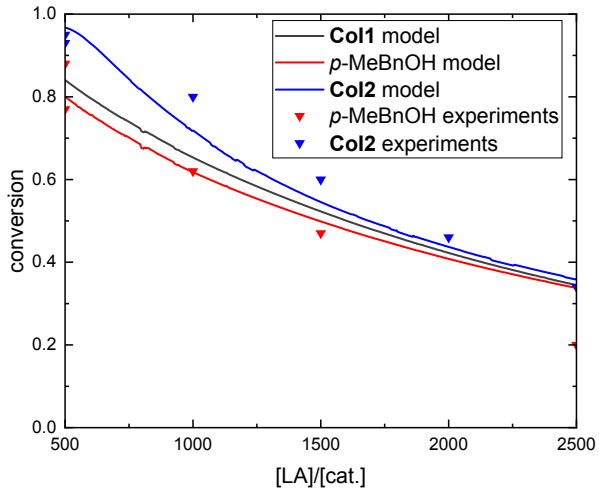

Figure 10: Influence of catalyst concentration for fixed co-I to catalyst ratio ([co-I]/[Cat] = 5/1) on conversion after 90 minutes for all co-Is. Experimental data for *p*-MeBnOH are taken from Conen et al.[87] and Fuchs[89].

By expanding the existing model to include catalysis of the reaction by catalyst residues and implementing bi-functional co-Is, further steps have been taken towards a deeper understanding of the kinetics of ROP with "asme" type catalysts. Using a bi-functional co-I, an additional step towards the potential establishment of non-toxic zinc catalysts for industrial polymerizations has been undertaken. The model-based analysis has significantly contributed to the understanding of the chemical relationships and allows conclusions to be drawn about conditions under which bi-functional co-Is can offer particularly large improvements over monofunctional co-Is.

These insights are essential for a successful scale-up in transitioning non-toxic catalysts from academic research to industrial application. The experimental study and model-based analysis presented here serve as an important tool for developing a catalyst-co-I system to replace the industrial catalyst tin octoate for a fully sustainable ROP of lactide.

Conclusions

The application of “asme”-type zinc guanidine carboxylate catalysts in the ROP of PLA has been extended to systematically investigate the influence of bifunctional co-initiators. In this study, 1,4-benzenedimethanol was evaluated as a bifunctional co-initiator and benchmarked against the monofunctional counterparts 1-hexanol and *p*-methylbenzyl alcohol. A variety of batch polymerizations were performed using different ratios of lactide to catalyst (ranging from 500:1 to 1500:1) and co-initiator equivalents (from 1 to 10 with respect to catalyst concentration). Polymerization progress and resulting polymer properties *X*, M_n and *Đ* were monitored using in situ Raman spectroscopy, NMR spectroscopy and GPC.

Our findings show that the use of both mono- and bi-functional co-initiators enables improved control over key polymer properties compared to reactions carried out in the absence of any co-initiator. Increasing the co-initiator concentration generally accelerates the polymerization kinetics, although a plateau in reaction rate is observed beyond a certain threshold. Our previously established kinetic model for the ROP of PLA was expanded to incorporate two critical mechanistic features: (1) the retained catalytic activity of the metal center after ligand dissociation and (2) an additional activation step required for bifunctional co-initiators.

Model predictions for *X* and *Đ* show generally good agreement with experimental results. However, some deviations for M_n were noted. The extended model was also used to predict polymerization behavior under conditions not used for parameter fitting, serving as validation. In these cases, both mono- and bi-functional systems exhibited good predictive accuracy,

Open Access Article. Published on 22 July 2025. Downloaded on 8/14/2025 4:27:06 AM.
This article is licensed under a Creative Commons Attribution 3.0 Unported Licence.

Faraday Discussions Accepted Manuscript

particularly in reproducing conversion and dispersity. Notably, bi-functional co-initiators led to higher conversion overall and are particularly suitable for application with “asme”-type catalysts by reducing the chain initiation by the ligand. Furthermore, at low co-initiator concentrations, catalysis by the deteriorated catalyst becomes increasingly relevant, emphasizing the importance of the model extension introduced in this work.

View Article Online
DOI: 10.1039/D5FD00062A

These findings highlight the versatility of the kinetic model and its applicability in tailoring ROP conditions through judicious choice of co-initiator type and concentration. Ultimately, this contributes to a deeper understanding of zinc guanidine carboxylate-catalyzed ROP while minimizing the experimental effort and paves the way for more efficient and tunable catalyst systems aimed at producing PLA with desired properties under industrially relevant conditions in larger scale.

Conflicts of interest

The authors declare no conflict of interest.

Data availability

The data that supports the findings of this study are openly available in RADAR4chem at

https://www.radar-service.eu/radar/en/dataset/qg2e8yckr7kjtj5b?token=cilcXLyzxVecDszreuQy

Acknowledgements

The authors than the Volkswagen foundation for funding the CIRCON project. The authors thank Total Corbion PLA for lactide donations. Furthermore, the authors would like to thank Prof Dr. Andrij Pich and Marion Conolly from DWI Leibniz Institute Aachen for MALDI Measurements. The authors would further like to thank RADAR4Chem for support and funding of the repository. The open access funding is enabled and organized by Projekt DEAL.

Notes and references

1 S. D. Anuar Sharuddin, F. Abnisa, W. M. A. Wan Daud and M. K. Aroua, *Energy Convers. Manage.*, 2016, **115**, 308–326.
2 N. S. Gurgacz, K. Kvale, M. Eby and A. J. Weaver, *FACETS*, 2023, **8**, 1–7.
3 C. M. C. Richard, E. Dejoie, C. Wiegand, G. Gouesbet, H. Colinet, P. Balzani, D. Siaussat and D. Renault, *J. Hazard. Mater.*, 2024, **477**, 135299.
4 J. N. Hahladakis, *Environ. Sci. Pollut. Res.*, 2020, **27**, 12830–12837.
5 T. Iwata, *Angew. Chem. Int. Ed.*, 2015, **54**, 3210–3215.
6 A. Jayakumar, S. Radoor, S. Siengchin, G. H. Shin and J. T. Kim, *Sci. Total Environ.*, 2023, **878**, 163156.
7 R. E. Drumright, P. R. Gruber and D. E. Henton, *Adv. Mater.*, 2000, **12**, 1841–1846.
8 M. J. Stanford and A. P. Dove, *Chem. Soc. Rev.*, 2010, **39**, 486–494.
9 P. McKeown and M. Jones, *Sustain. Chem.*, 2020, **1**, 1–22.
10 S. Jacobsen, H. G. Fritz, P. Degée, P. Dubois and R. Jérôme, *Polym. Eng. Sci.*, 1999, **39**, 1311–1319.
11 O. Dechy-Cabaret, B. Martin-Vaca and D. Bourissou, *Chem. Rev.*, 2004, **104**, 6147–6176.
12 A. Stjerndahl, A. Finne-Wistrand, A.-C. Albertsson, C. M. Bäckesjö and U. Lindgren, *J. Biomed. Mater. Res. Part A*, 2008, **87**, 1086–1091.
13 A. Stjerndahl, A. F. Wistrand and A.-C. Albertsson, *Biomacromolecules*, 2007, **8**, 937–940.

Open Access Article. Published on 22 July 2025. Downloaded on 8/14/2025 4:27:06 AM.
This article is licensed under a Creative Commons Attribution 3.0 Unported Licence.

Faraday Discussions Accepted Manuscript

View Article Online
DOI: 10.1039/D5FD00062A

14 A. Buchard, R. H. Platel, A. Auffrant, X. F. Le Goff, P. Le Floch and C. K. Williams, *Organometallics*, 2010, **29**, 2892–2900.
15 N. Yuntawattana, T. M. McGuire, C. B. Durr, A. Buchard and C. K. Williams, *Catal. Sci. Technol.*, 2020, **10**, 7226–7239.
16 F. Fiorentini, W. T. Diment, A. C. Deacy, R. W. F. Kerr, S. Faulkner and C. K. Williams, *Nat Commun*, 2023, **14**, 4783.
17 C. Bakewell, A. J. P. White, N. J. Long and C. K. Williams, *Angew. Chem. Int. Ed.*, 2014, **53**, 9226–9230.
18 J. Y. C. Lim, N. Yuntawattana, P. D. Beer and C. K. Williams, *Angew. Chem.*, 2019, **131**, 6068–6072.
19 A. J. Chmura, M. G. Davidson, M. D. Jones, M. D. Lunn, M. F. Mahon, A. F. Johnson, P. Khunkamchoo, S. L. Roberts and S. S. F. Wong, *Macromolecules*, 2006, **39**, 7250–7257.
20 A. J. Chmura, D. M. Cousins, M. G. Davidson, M. D. Jones, M. D. Lunn and M. F. Mahon, *Dalton Trans.*, 2008, 1437–1443.
21 A. Buchard, M. G. Davidson, G. Du Gobius Sart, M. D. Jones, G. Kociok-Köhn, S. N. McCormick and P. McKeown, *Inorg. Chem.*, 2024, **63**, 27–38.
22 O. J. Driscoll, C. K. C. Leung, M. F. Mahon, P. McKeown and M. D. Jones, *Eur. J. Inorg. Chem.*, 2018, **2018**, 5129–5135.
23 J. A. Stewart, P. McKeown, O. J. Driscoll, M. F. Mahon, B. D. Ward and M. D. Jones, *Macromolecules*, 2019, **52**, 5977–5984.
24 J. Beament, M. F. Mahon, A. Buchard and M. D. Jones, *Organometallics*, 2018, **37**, 1719–1724.
25 M. D. Jones, L. Brady, P. McKeown, A. Buchard, P. M. Schäfer, L. H. Thomas, M. F. Mahon, T. J. Woodman and J. P. Lowe, *Chemical science*, 2015, **6**, 5034–5039.
26 J.-C. Buffet and J. Okuda, *Chem Commun (Camb)*, 2011, **47**, 4796–4798.
27 R. Rittinghaus, P. M. Schäfer, P. Albrecht, C. Conrads, A. Hoffmann, A. N. Ksiazkiewicz, O. Bienemann, A. Pich and S. Herres-Pawlis, *ChemSusChem*, 2019, **12**, 2161–2165.
28 R. Rittinghaus, A. Karabulut, A. Hoffmann and S. Herres-Pawlis, *Angew. Chem. Int. Ed.*, 2021, **60**, 21795–21800.
29 S. Herres-Pawlis, R. Rittinghaus, J. Zenner, A. Pich and M. Kol, *Angew. Chem. Int. Ed.*, 2022.
30 P. McKeown, S. N. McCormick, M. F. Mahon and M. Jones, *Polym. Chem.*, 2018, **9**, 5339–5347.
31 A. J. Chmura, M. G. Davidson, C. J. Frankis, M. Jones and M. D. Lunn, *Chem Commun (Camb)*, 2008, 1293–1295.
32 F. Santulli, I. D'Auria, L. Boggioni, S. Losio, M. Proverbio, C. Costabile and M. Mazzeo, *Organometallics*, 2020, **39**, 1213–1220.
33 P. McKeown, M. G. Davidson, G. Kociok-Köhn and M. D. Jones, *Chem Commun (Camb)*, 2016, **52**, 10431–10434.
34 O. J. Driscoll, C. H. Hafford-Tear, P. McKeown, J. A. Stewart, G. Kociok-Köhn, M. F. Mahon and M. D. Jones, *Dalton Trans.*, 2019, **48**, 15049–15058.
35 P. V. S. Nylund, B. Monney, C. Weder and M. Albrecht, *Catal. Sci. Technol.*, 2022, **12**, 996–1004.
36 H. Shere, P. McKeown, M. F. Mahon and M. D. Jones, *Eur. Polym. J.*, 2019, **114**, 319–325.
37 V. Vaillant-Coindard, B. Théron, G. Printz, F. Chotard, C. Balan, Y. Rousselin, P. Richard, I. Tolbatov, P. Fleurat-Lessard, E. Bodio, R. Malacea-Kabbara, J. Bayardon, S. Dagorne and P. Le Gendre, *Organometallics*, 2022, **41**, 2920–2932.
38 A. J. Chmura, C. J. Chuck, M. G. Davidson, M. D. Jones, M. D. Lunn, S. D. Bull and M. F. Mahon, *Angew. Chem.*, 2007, **119**, 2330–2333.
39 A. Finne, Reema and A.-C. Albertsson, *J. Polym. Sci. A Polym. Chem.*, 2003, **41**, 3074–3082.

Open Access Article. Published on 22 July 2025. Downloaded on 8/14/2025 4:27:06 AM.
This article is licensed under a Creative Commons Attribution 3.0 Unported Licence.

Faraday Discussions Accepted Manuscript

View Article Online
DOI: 10.1039/D5FD00062A

40 H. Ma, T. P. Spaniol and J. Okuda, *Angew. Chem.*, 2006, **118**, 7982–7985.
41 B. J. Jeffery, E. L. Whitelaw, D. Garcia-Vivo, J. A. Stewart, M. F. Mahon, M. G. Davidson and M. D. Jones, *Chem Commun (Camb)*, 2011, **47**, 12328–12330.
42 A. Sauer, A. Kapelski, C. Fliedel, S. Dagorne, M. Kol and J. Okuda, *Dalton Trans.*, 2013, **42**, 9007–9023.
43 S. L. Hancock, M. F. Mahon and M. D. Jones, *Dalton Trans.*, 2013, **42**, 9279–9285.
44 C. Romain, Y. Zhu, P. Dingwall, S. Paul, H. S. Rzepa, A. Buchard and C. K. Williams, *J. Am. Chem. Soc.*, 2016, **138**, 4120–4131.
45 A. D. Schwarz, A. L. Thompson and P. Mountford, *Inorg. Chem.*, 2009, **48**, 10442–10454.
46 M. D. Jones, M. G. Davidson, C. G. Keir, L. M. Hughes, M. F. Mahon and D. C. Apperley, *Eur. J. Inorg. Chem.*, 2009, **2009**, 635–642.
47 S. Ghosh, Y. Schulte, C. Wölper, A. Tjaberings, A. H. Gröschel, G. Haberhauer and S. Schulz, *Organometallics*, 2022, **41**, 2698–2708.
48 H. Shere, P. McKeown, M. F. Mahon and M. D. Jones, *Eur. Polym. J.*, 2019, **114**, 319–325.
49 A. Thevenon, C. Romain, M. S. Bennington, A. J. P. White, H. J. Davidson, S. Brooker and C. K. Williams, *Angew. Chem. Int. Ed.*, 2016, **55**, 8680–8685.
50 M. Fuchs, S. Schmitz, P. M. Schäfer, T. Secker, A. Metz, A. N. Ksiazkiewicz, A. Pich, P. Kögerler, K. Y. Monakhov and S. Herres-Pawlis, *Eur. Polym. J.*, 2020, **122**, 109302.
51 A. Hermann, S. Hill, A. Metz, J. Heck, A. Hoffmann, L. Hartmann and S. Herres-Pawlis, *Angew. Chem. Int. Ed.*, 2020, **59**, 21778–21784.
52 T. Rosen, Y. Popowski, I. Goldberg and M. Kol, *Chemistry – A European Journal*, 2016, **22**, 11533–11536.
53 M. Honrado, A. Otero, J. Fernández-Baeza, L. F. Sánchez-Barba, A. Garcés, A. Lara-Sánchez and A. M. Rodríguez, *Organometallics*, 2014, **33**, 1859–1866.
54 M. Honrado, S. Sobrino, J. Fernández-Baeza, L. F. Sánchez-Barba, A. Garcés, A. Lara-Sánchez and A. M. Rodríguez, *Chem Commun (Camb)*, 2019, **55**, 8947–8950.
55 A. Metz, R. Plothe, B. Glowacki, A. Koszalkowski, M. Scheckenbach, A. Beringer, T. Rösener, J. Michaelis de Vasconcellos, R. Haase, U. Flörke, A. Hoffmann and S. Herres-Pawlis, *Eur. J. Inorg. Chem.*, 2016, **2016**, 4974–4987.
56 C. Fliedel, V. Rosa, F. M. Alves, A. M. Martins, T. Avilés and S. Dagorne, *Dalton Trans.*, 2015, **44**, 12376–12387.
57 E. D. Akpan, S. O. Ojwach, B. Omondi and V. O. Nyamori, *Polyhedron*, 2016, **110**, 63–72.
58 C. K. Williams, L. E. Breyfogle, S. K. Choi, W. Nam, Young,, Victor G., M. A. Hillmyer and W. B. Tolman, *J. Am. Chem. Soc.*, 2003, **125**, 11350–11359.
59 C. C. Roberts, B. R. Barnett, D. B. Green and J. M. Fritsch, *Organometallics*, 2012, **31**, 4133–4141.
60 D. Jędrzkiewicz, G. Adamus, M. Kwiecień, Ł. John and J. Ejfler, *Inorg. Chem.*, 2017, **56**, 1349–1365.
61 A. Otero, J. Fernández-Baeza, L. F. Sánchez-Barba, S. Sobrino, A. Garcés, A. Lara-Sánchez and A. M. Rodríguez, *Dalton Trans.*, 2017, **46**, 15107–15117.
62 N. M. Rezayee, K. A. Gerling, A. L. Rheingold and J. M. Fritsch, *Dalton Trans.*, 2013, **42**, 5573–5586.
63 Z. Dai, J. Zhang, Y. Gao, N. Tang, Y. Huang and J. Wu, *Catal. Sci. Technol.*, 2013, **3**, 3268.
64 D. J. Darensbourg and O. Karroonnirun, *Macromolecules*, 2010, **43**, 8880–8886.
65 C. Fliedel, D. Vila-Viçosa, M. J. Calhorda, S. Dagorne and T. Avilés, *ChemCatChem*, 2014, **6**, 1357–1367.
66 Y. Sun, Y. Cui, J. Xiong, Z. Dai, N. Tang and J. Wu, *Dalton Trans.*, 2015, **44**, 16383–16391.
67 J. E. Chellali, A. K. Alverson and J. R. Robinson, *ACS Catal.*, 2022, **12**, 5585–5594.

Open Access Article. Published on 22 July 2025. Downloaded on 8/14/2025 4:27:06 AM.
This article is licensed under a Creative Commons Attribution 3.0 Unported Licence.

Faraday Discussions Accepted Manuscript

View Article Online
DOI: 10.1039/D5FD00062A

68 P. McKeown, J. Brown-Humes, M. G. Davidson, M. F. Mahon, T. J. Woodman and M. D. Jones, *Dalton Trans.*, 2017, **46**, 5048–5057.
69 S. P. Bassett, A. D. Russell, P. McKeown, I. Robinson, T. R. Forder, V. Taresco, M. G. Davidson and S. M. Howdle, *Green Chem.*, 2020, **22**, 2197–2202.
70 S. Ghosh, P. M. Schäfer, D. Dittrich, C. Scheiper, P. Steiniger, G. Fink, A. N. Ksiazkiewicz, A. Tjaberings, C. Wölper, A. H. Gröschel, A. Pich, S. Herres-Pawlis and S. Schulz, *ChemistryOpen*, 2019, **8**, 951–960.
71 P. Steiniger, P. M. Schäfer, C. Wölper, J. Henkel, A. N. Ksiazkiewicz, A. Pich, S. Herres-Pawlis and S. Schulz, *Eur. J. Inorg. Chem.*, 2018, **2018**, 4014–4021.
72 Z. Zhong, P. J. Dijkstra and J. Feijen, *Angew. Chem.*, 2002, **114**, 4692–4695.
73 A. Hermann, T. Becker, M. A. Schäfer, A. Hoffmann and S. Herres-Pawlis, *ChemSusChem*, 2022, **15**, e202201075.
74 P. M. Schäfer, M. Fuchs, A. Ohligschläger, R. Rittinghaus, P. McKeown, E. Akin, M. Schmidt, A. Hoffmann, M. A. Liauw, M. Jones and S. Herres-Pawlis, *ChemSusChem*, 2017, **10**, 3547–3556.
75 P. M. Schäfer, P. McKeown, M. Fuchs, R. Rittinghaus, A. Hermann, J. Henkel, S. Seidel, C. Roitzheim, A. N. Ksiazkiewicz, A. Hoffmann, A. Pich, M. Jones and S. Herres-Pawlis, *Dalton Trans.*, 2019, **48**, 6071–6082.
76 P. M. Schäfer and S. Herres-Pawlis, *ChemPlusChem*, 2020, **85**, 1044–1052.
77 K. A. George, F. Schué, T. V. Chirila and E. Wentrup-Byrne, *J. Polym. Sci. A Polym. Chem.*, 2009, **47**, 4736–4748.
78 A. Amgoune, C. M. Thomas and J.-F. Carpentier, *Macromol. Rapid Commun.*, 2007, **28**, 693–697.
79 R. D. Rittinghaus, J. Zenner, A. Pich, M. Kol and S. Herres-Pawlis, *Angew. Chem. Int. Ed.*, 2022, **61**, e202112853.
80 B. Théron, V. Vaillant-Coindard, C. Balan, Y. Rousselin, J. Bayardon, R. Malacea-Kabbara and P. Le Gendre, *Dalton Trans.*, 2023, **52**, 7854–7868.
81 J. Payne, P. McKeown, M. F. Mahon, E. A. C. Emanuelsson and M. Jones, *Polym. Chem.*, 2020, **11**, 2381–2389.
82 S. D'Aniello, S. Laviéville, F. Santulli, M. Simon, M. Sellitto, C. Tedesco, C. M. Thomas and M. Mazzeo, *Catal. Sci. Technol.*, 2022, **12**, 6142–6154.
83 D. Bandelli, C. Weber and U. S. Schubert, *Macromol. Rapid Commun.*, 2019, **40**, e1900306.
84 T. Rosen, I. Goldberg, W. Navarra, V. Venditto and M. Kol, *Angew. Chem. Int. Ed.*, 2018, **57**, 7191–7195.
85 R. Hador, M. Shuster, V. Venditto and M. Kol, *Angew. Chem. Int. Ed.*, 2022, **61**, e202207652.
86 Y. Zhou, G. S. Nichol and J. A. Garden, *Eur. J. Inorg. Chem.*, 2022, **2022**, e202200134.
87 N. Conen, M. Fuchs, A. Hoffmann, S. Herres-Pawlis and A. Jupke, *Adv. Sustain. Syst.*, 2023, 2200359.
88 A. Kowalski, A. Duda and S. Penczek, *Macromolecules*, 1998, **31**, 2114–2122.
89 M. Fuchs, RWTH Aachen University, 2024.
90 G. Schwach, J. Coudane, R. Engel and M. Vert, *Polym. Bull.*, 1996, **37**, 771–776.
91 Y. Yu, E. J. Fischer, G. Storti and M. Morbidelli, *Ind. Eng. Chem. Res.*, 2014, **53**, 7333–7342.
92 Y. Yu, G. Storti and M. Morbidelli, *Macromolecules*, 2009, **42**, 8187–8197.
93 Y. Yu, G. Storti and M. Morbidelli, *Ind. Eng. Chem. Res.*, 2011, **50**, 7927–7940.
94 S. Metkar, V. Sathe, I. Rahman, B. Idage and S. Idage, *Chem. Eng. Commun.*, 2019, **206**, 1159–1167.
95 P. Pladis, K. Karidi, T. Mantourlias and C. Kiparissides, *Macromol. React. Eng.*, 2014, **8**, 813–825.

Open Access Article. Published on 22 July 2025. Downloaded on 8/14/2025 4:27:06 AM.
This article is licensed under a Creative Commons Attribution 3.0 Unported Licence.

Faraday Discussions Accepted Manuscript

96 F. Weng, X. Li, Y. Wang, W.-J. Wang and S. J. Severtson, *Macromol. React. Eng.*, 2015, **9**, 535–544.
97 A. Zubov and G. Sin, *Chem. Eng. J.*, 2018, **336**, 361–375.
98 D. R. Witzke, Michigan State University, 1997.
99 H. M. Hulburt and S. Katz, *Chem. Eng. Sci.*, 1964, **19**, 555–574.
100 R. P. Rosa, F. V. Ferreira and L. M.F. Lona, *Chem. Eng. Sci.*, 2021, **246**, 116934.
101 I. Zapata-González and E. Saldívar-Guerra, *Can J Chem Eng*, 2023, **101**, 5324–5356.

View Article Online
DOI: 10.1039/D5FD00062A

Open Access Article. Published on 22 July 2025. Downloaded on 8/14/2025 4:27:06 AM.
This article is licensed under a Creative Commons Attribution 3.0 Unported Licence.

Faraday Discussions Accepted Manuscript